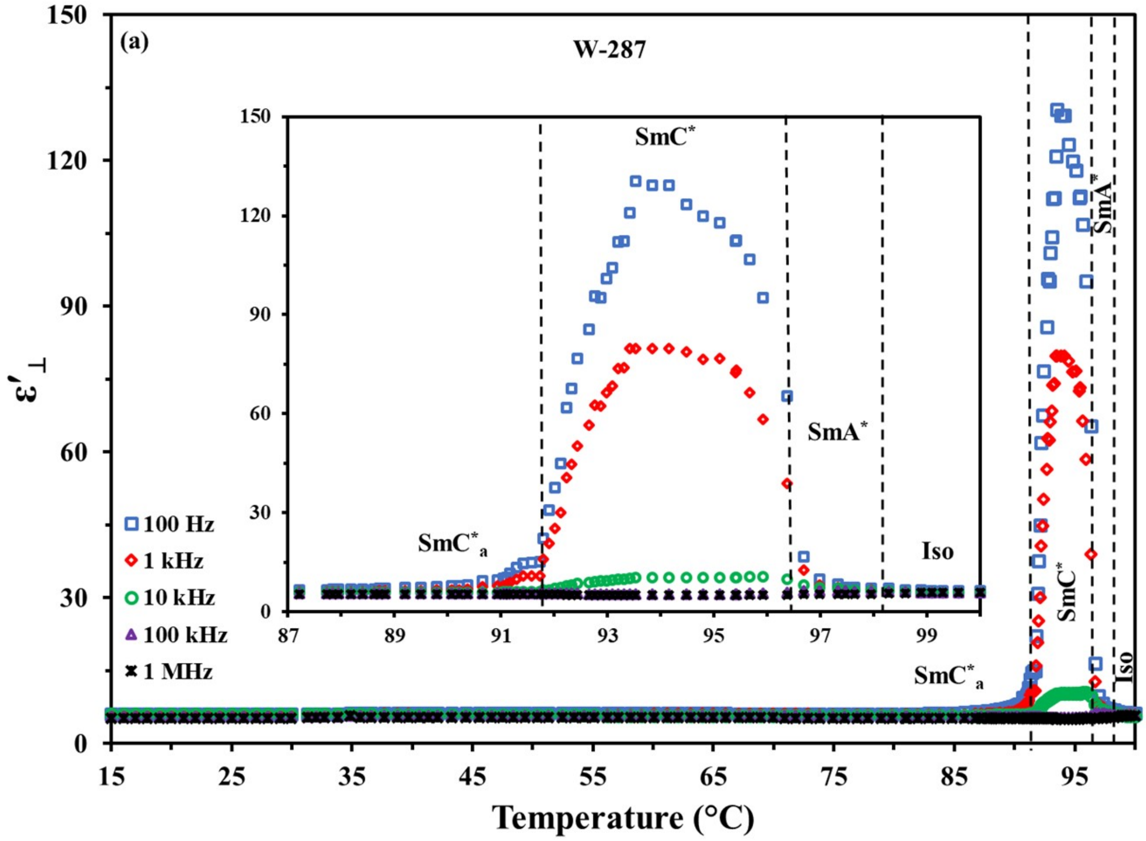
(a)
W-287
SmC*
SmA*
Iso
SmC*a
100 Hz
1 kHz
10 kHz
100 kHz
1 MHz
Temperature (°C)
ε'⊥

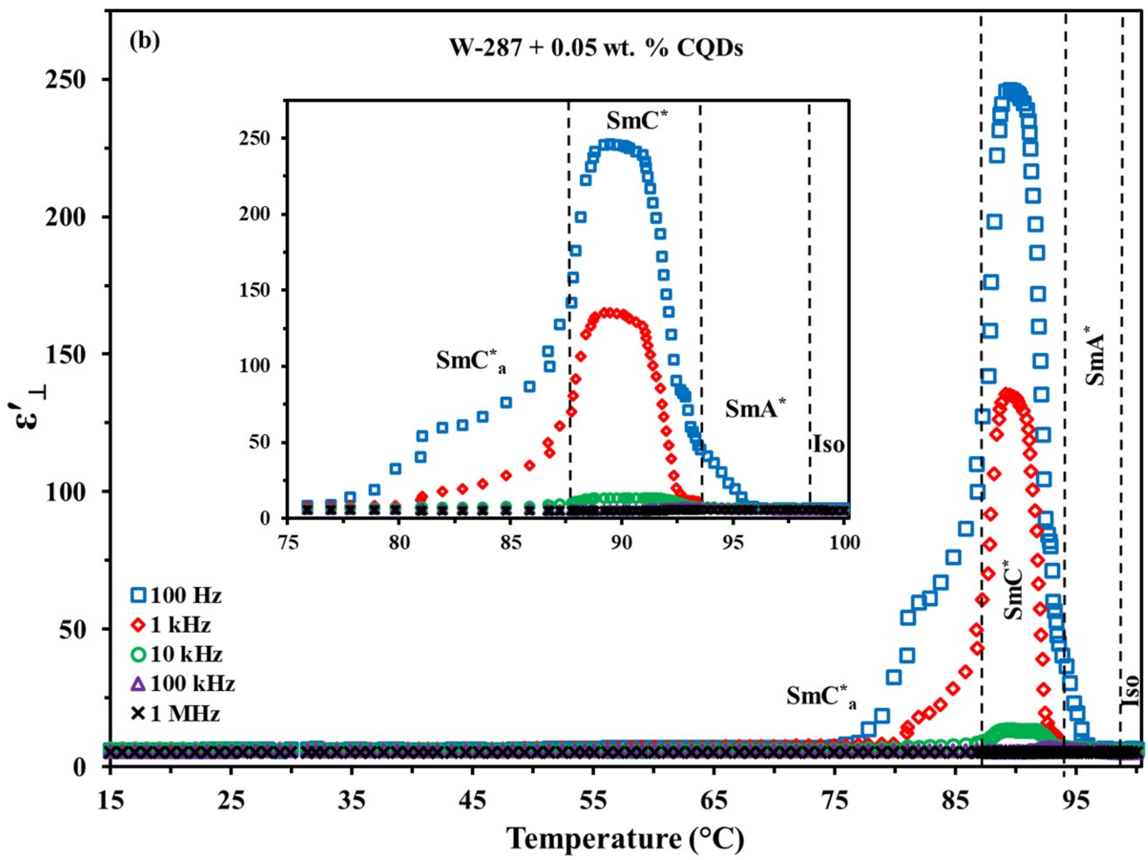
(b)
W-287 + 0.05 wt. % CQDs
SmC*
SmA*
Iso
SmC*a
100 Hz
1 kHz
10 kHz
100 kHz
1 MHz
Temperature (°C)
ε'⊥

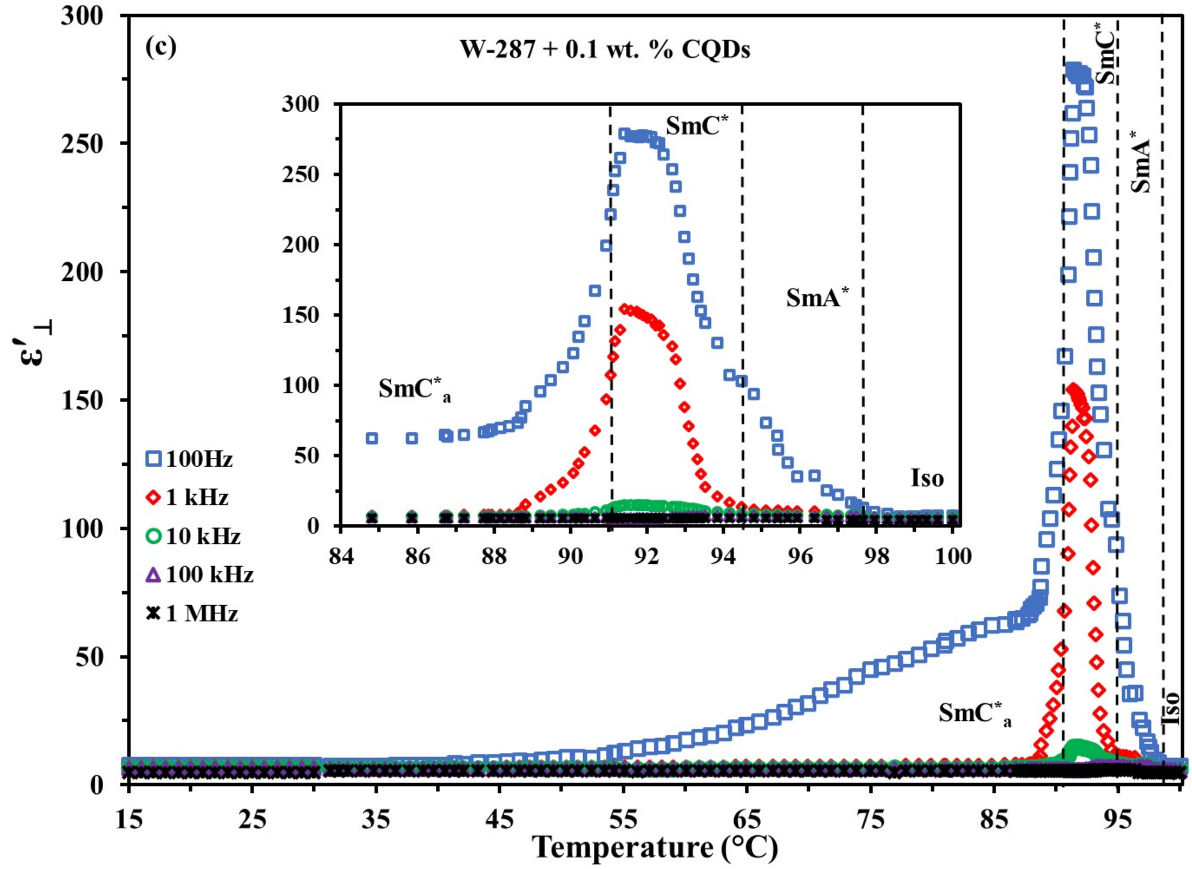

Figure S1. Temperature dependence of the $\varepsilon'_{\perp}$ at different frequencies (100 Hz, 1 kHz, 10 kHz, 100 kHz, and 1 MHz) in the cooling cycle of (a) pure W-287, (b) composite-1, and (c) composite-2. A higher value of $\varepsilon'_{\perp}$ in the (ferroelectric) SmC* phase differentiate it from SmC*$_a$ (antiferroelectric) phase (left) and the (paraelectric) SmA* phase (right). Insets show the enlarged view of the various phase transitions. Vertical dash lines show the transition temperatures based on DSC studies extrapolated at the scan rate of 0 °C/min.

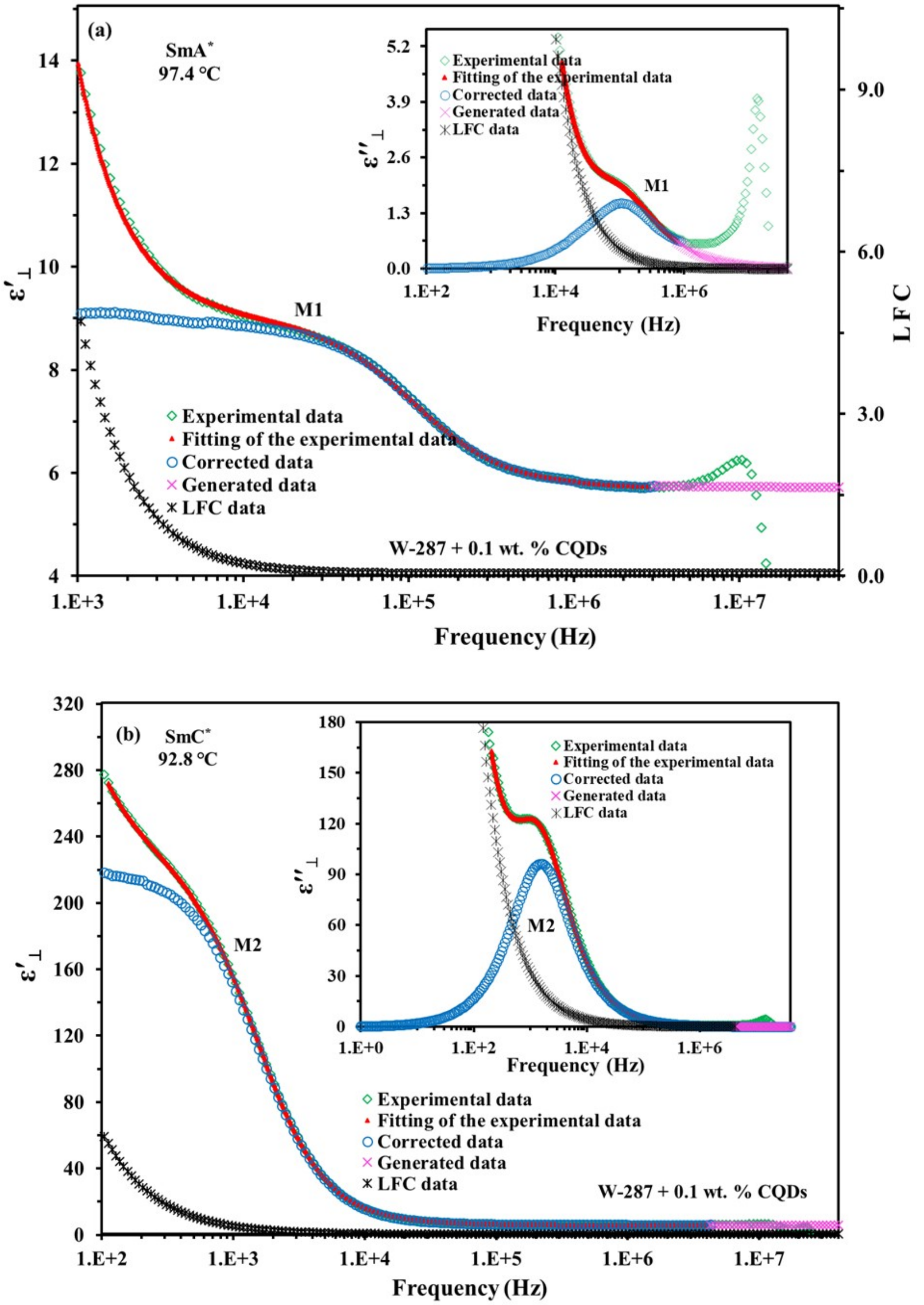

Figure S2. Dielectric relaxation spectra of the permittivity $(\varepsilon'_{\perp})$ and loss $(\varepsilon''_{\perp})$ of composite-2 in the (a) SmA* phase at 97.4 °C and, (b) SmC* phase at 92.8 °C exhibiting various relaxation modes. Curves show the experimental data (open rhombus), data obtained by fitting the experimental data (open triangle), corrected data (open circle), and generated data (cross). The corrected data have been extracted after subtracting the parasitic effects i.e. low-frequency (double cross) and high-frequency correction (plus sign) terms from the experimental data.

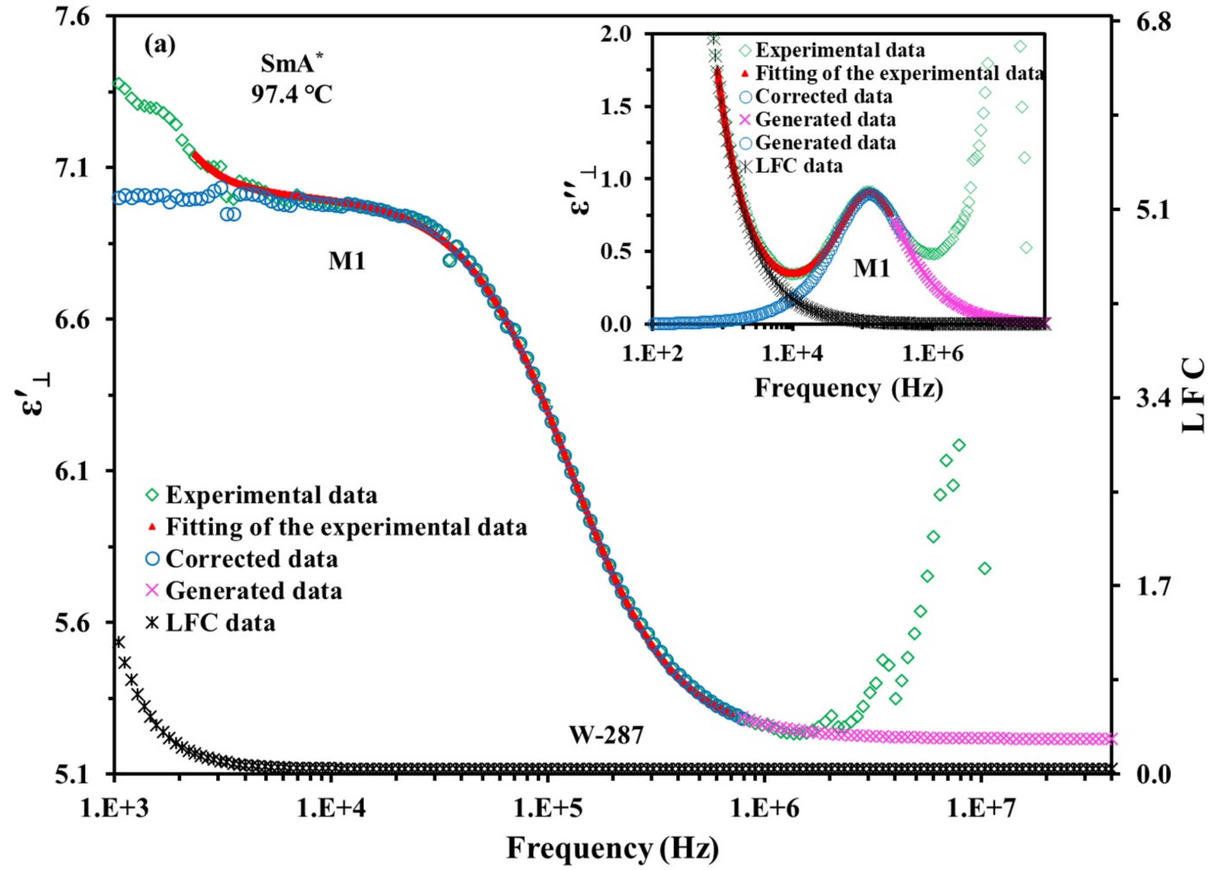

(a)
SmA*
97.4 °C
M1
W-287
ε′⊥
LFC
Frequency (Hz)
Experimental data
Fitting of the experimental data
Corrected data
Generated data
LFC data
7.6
7.1
6.6
6.1
5.6
5.1
6.8
5.1
3.4
1.7
0.0
1.E+3
1.E+4
1.E+5
1.E+6
1.E+7
ε″⊥
2.0
1.5
1.0
0.5
0.0
1.E+2
1.E+4
1.E+6
Experimental data
Fitting of the experimental data
Corrected data
Generated data
Generated data
LFC data
M1
Frequency (Hz)

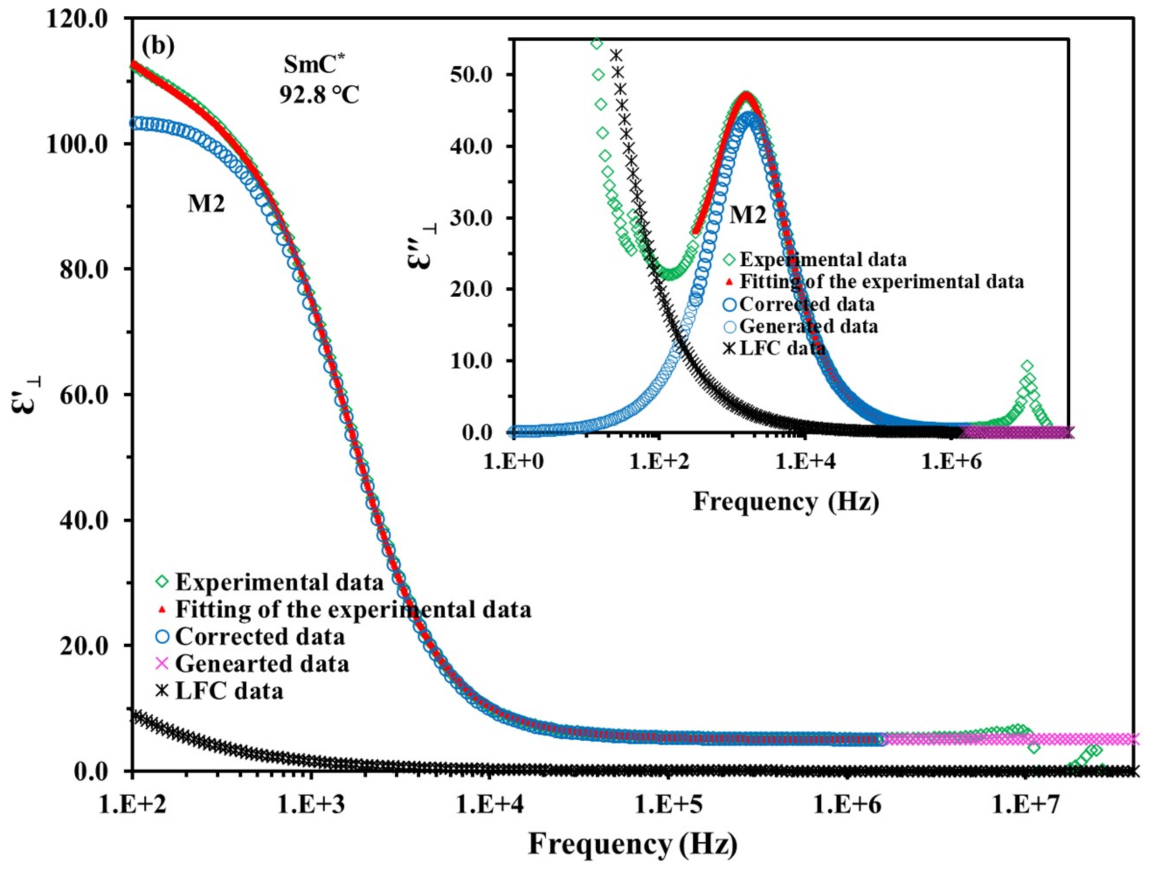

(b)
SmC*
92.8 °C
M2
ε′⊥
Frequency (Hz)
Experimental data
Fitting of the experimental data
Corrected data
Genearted data
LFC data
120.0
100.0
80.0
60.0
40.0
20.0
0.0
1.E+2
1.E+3
1.E+4
1.E+5
1.E+6
1.E+7
ε″⊥
50.0
40.0
30.0
20.0
10.0
0.0
1.E+0
1.E+2
1.E+4
1.E+6
M2
Experimental data
Fitting of the experimental data
Corrected data
Generated data
LFC data
Frequency (Hz)

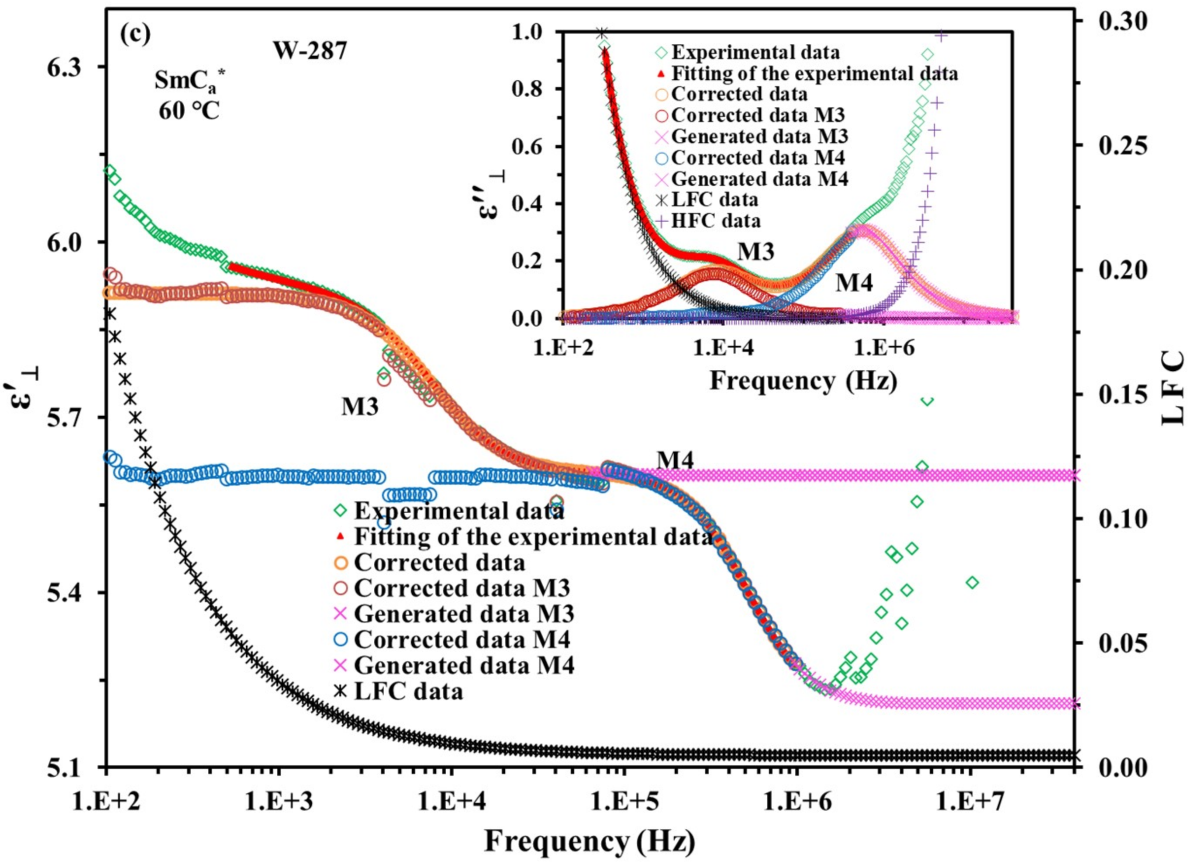

Figure S3. Dielectric relaxation spectra of the permittivity $(\varepsilon'_{\perp})$ and the inset shows a loss $(\varepsilon''_{\perp})$ of pure W-287 in the (a) SmA* phase at 97.4 °C (b) SmC* phase at 92.8 °C and, (c) SmC*$_a$ phase at 60 °C exhibiting relaxation modes. Curves show the experimental data (open rhombus), data obtained by fitting the experimental data (open triangle), corrected data (open circle), and generated data (cross). The corrected data have been extracted after subtracting the parasitic effects i.e. low-frequency (double cross) and high-frequency correction (plus sign) terms from the experimental data.

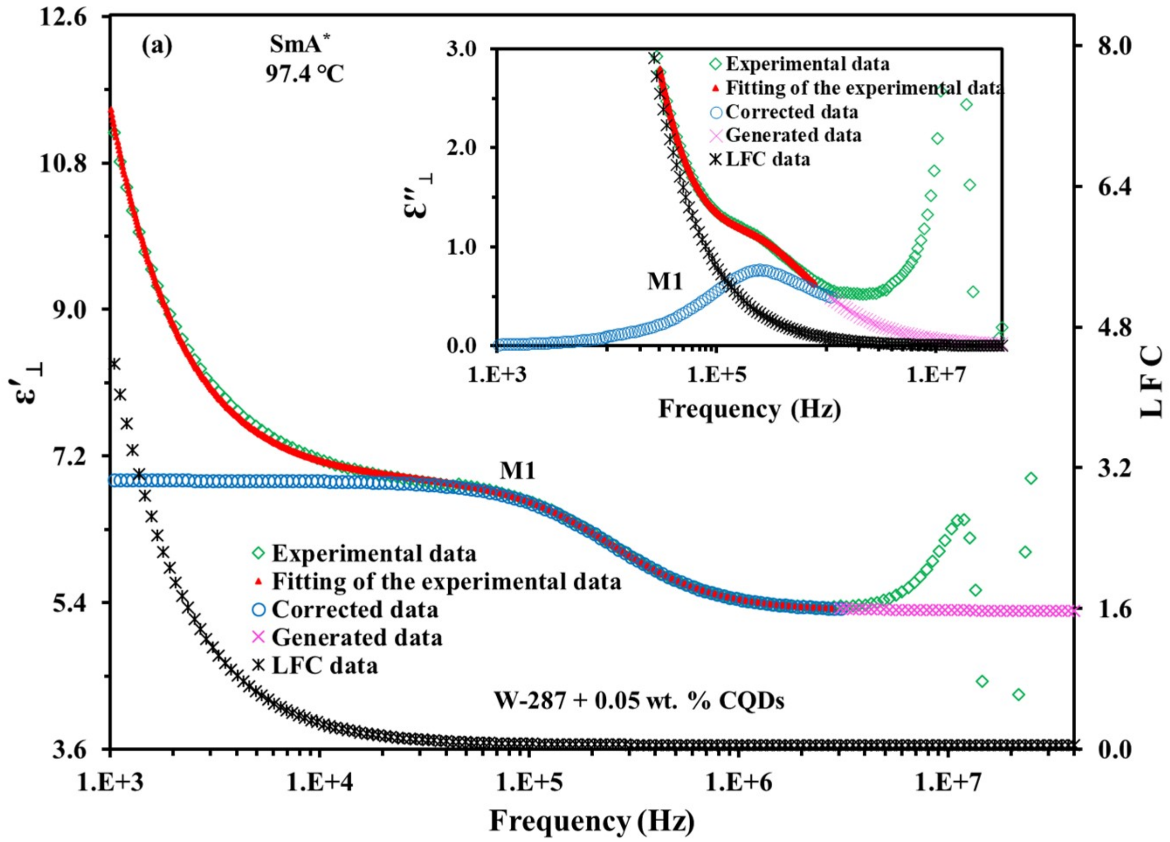

(a)
SmA*
97.4 °C
M1
Experimental data
Fitting of the experimental data
Corrected data
Generated data
LFC data
W-287 + 0.05 wt. % CQDs
Frequency (Hz)
LFC

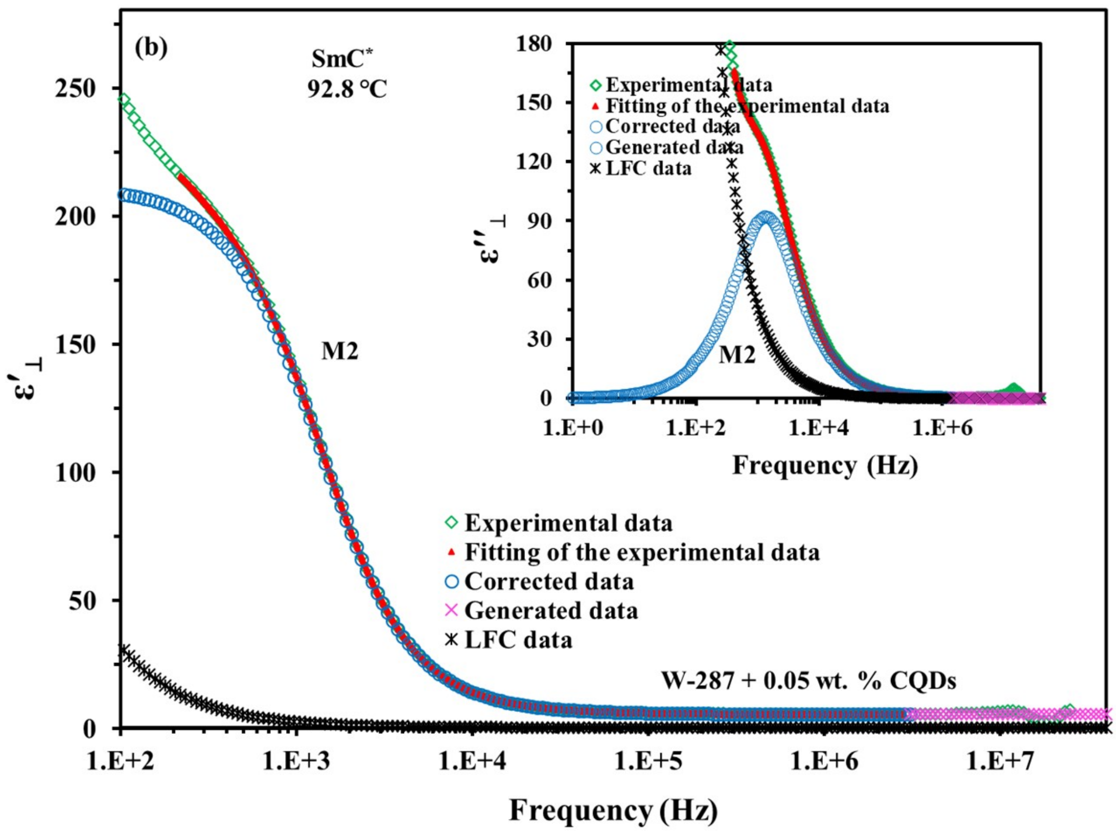

(b)
SmC*
92.8 °C
M2
Experimental data
Fitting of the experimental data
Corrected data
Generated data
LFC data
W-287 + 0.05 wt. % CQDs
Frequency (Hz)

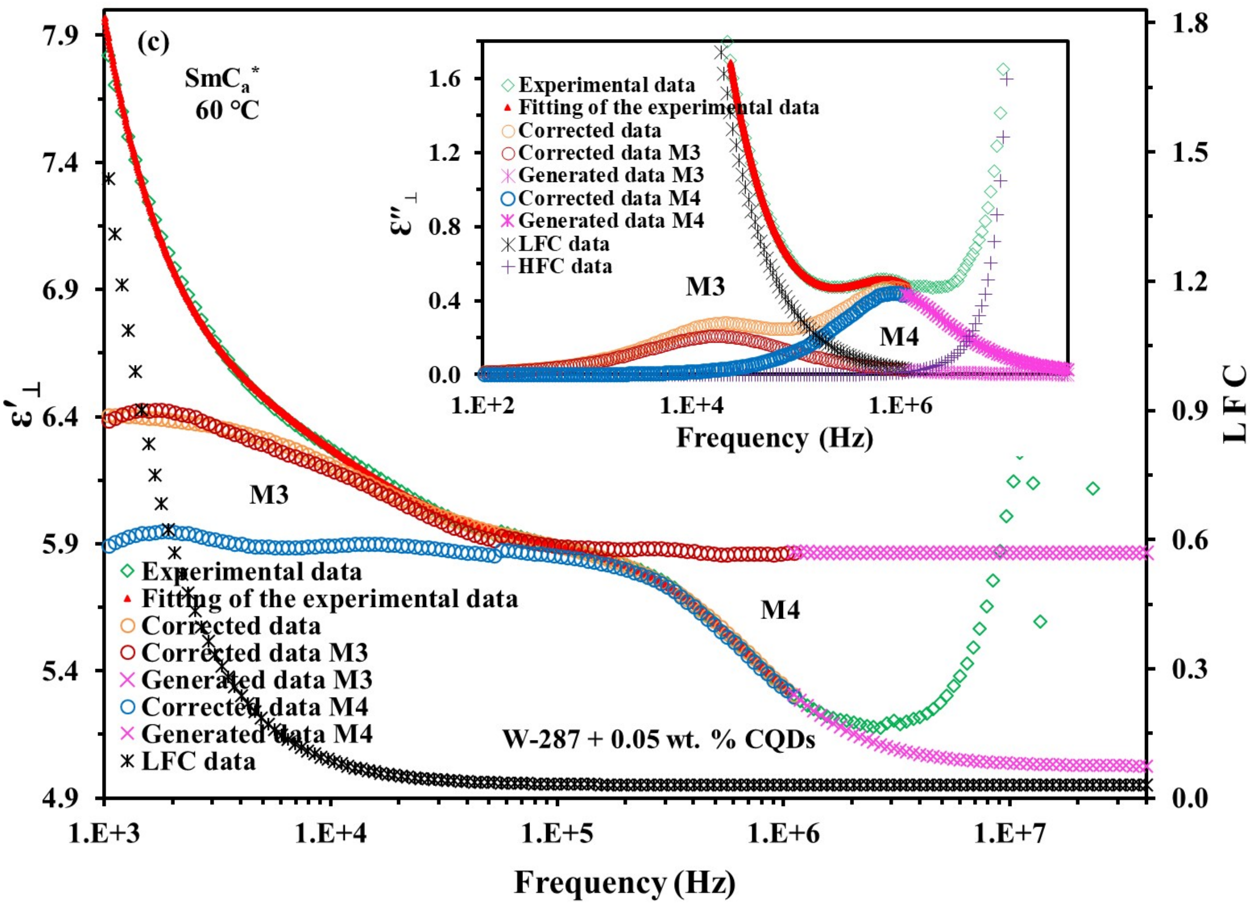

Figure S4. Dielectric relaxation spectra of the permittivity $(\varepsilon'_{\perp})$ and the inset shows a loss $(\varepsilon''_{\perp})$ of composite-1 in the (a) SmA* phase at 97.4 °C (b) SmC* phase at 92.8 °C and, (c) SmC*$_a$ phase at 60 °C exhibiting relaxation modes. Curves show the experimental data (open rhombus), data obtained by fitting the experimental data (open triangle), corrected data (open circle), and generated data (cross). The corrected data have been extracted after subtracting the parasitic effects i.e. low-frequency (double cross) and high-frequency correction (plus sign) terms from the experimental data.

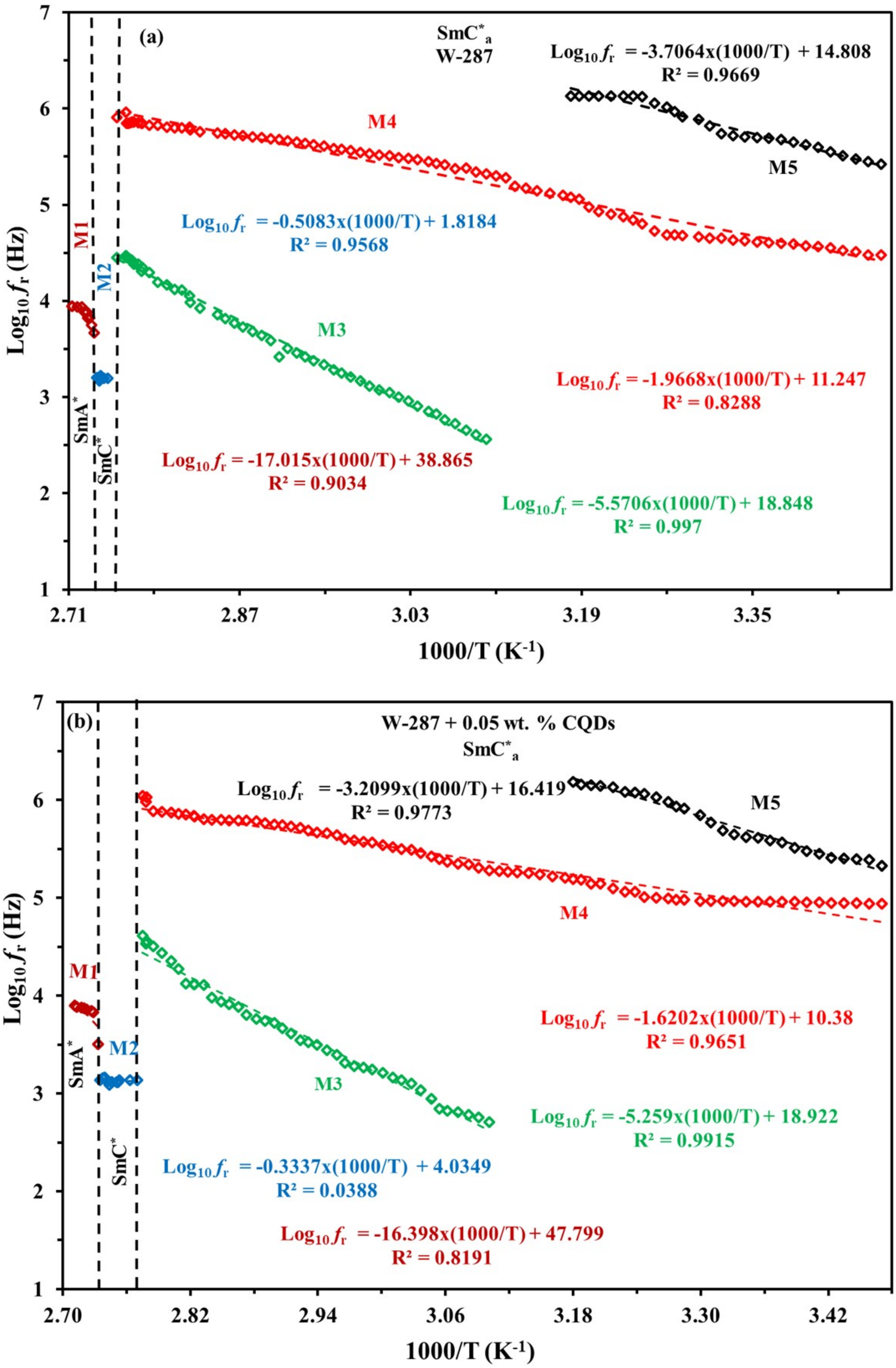

Figure S5. Temperature dependences of the relaxation frequencies (f_r) in Hz of various relaxation modes in different mesophases of (a) pure W-287 and, (b) composite-1. Vertical dash lines show the transition temperatures based on DSC studies extrapolated at the scan rate of 0 °C/min.

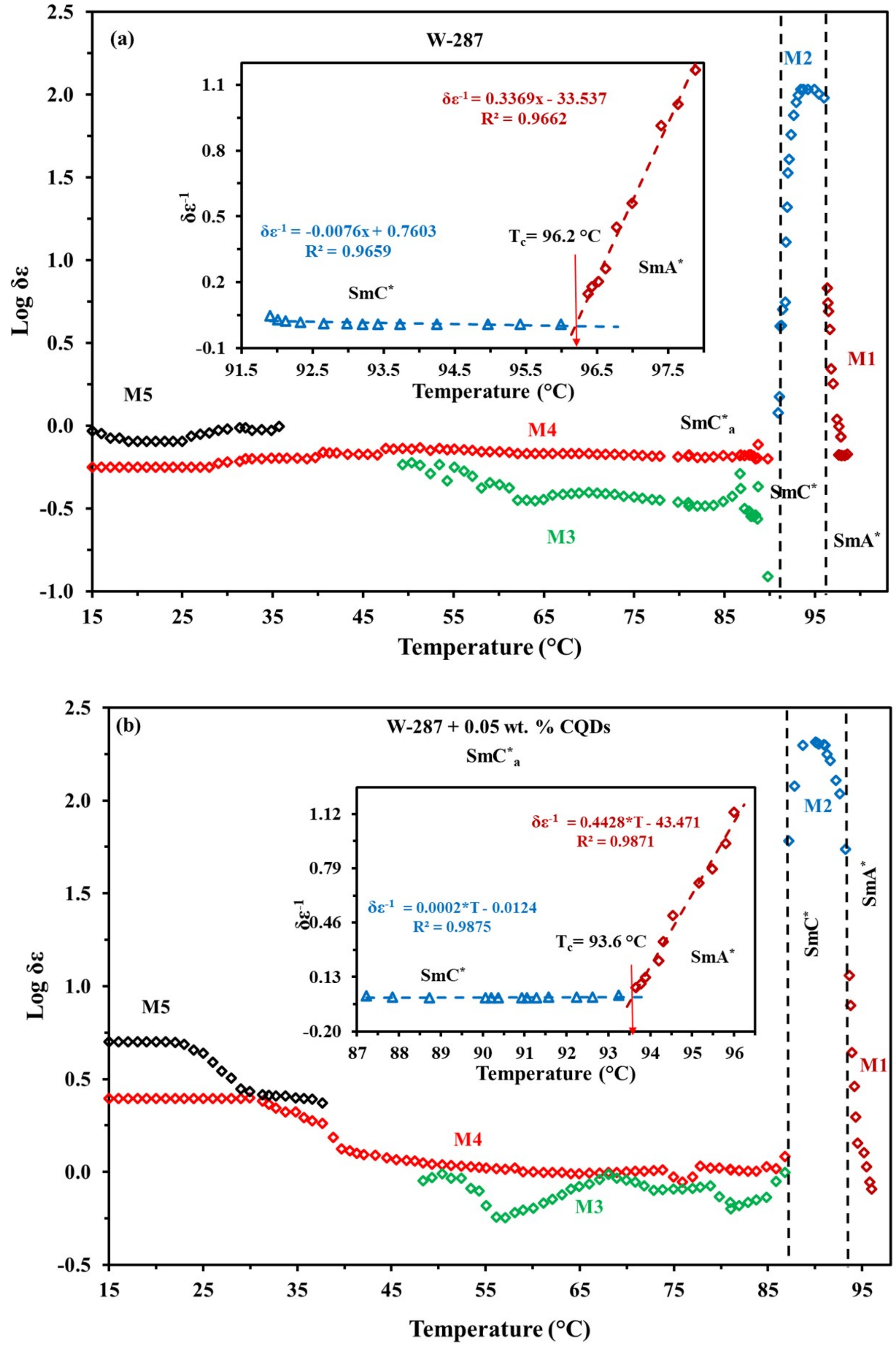

Figure S6. Temperature dependence of dielectric relaxation strength (δε) of various relaxation modes in different mesophases of (a) pure W-287 and, (b) composite-1. Vertical dash lines show the transition temperatures based on DSC studies extrapolated at the scan rate of 0 °C/min.

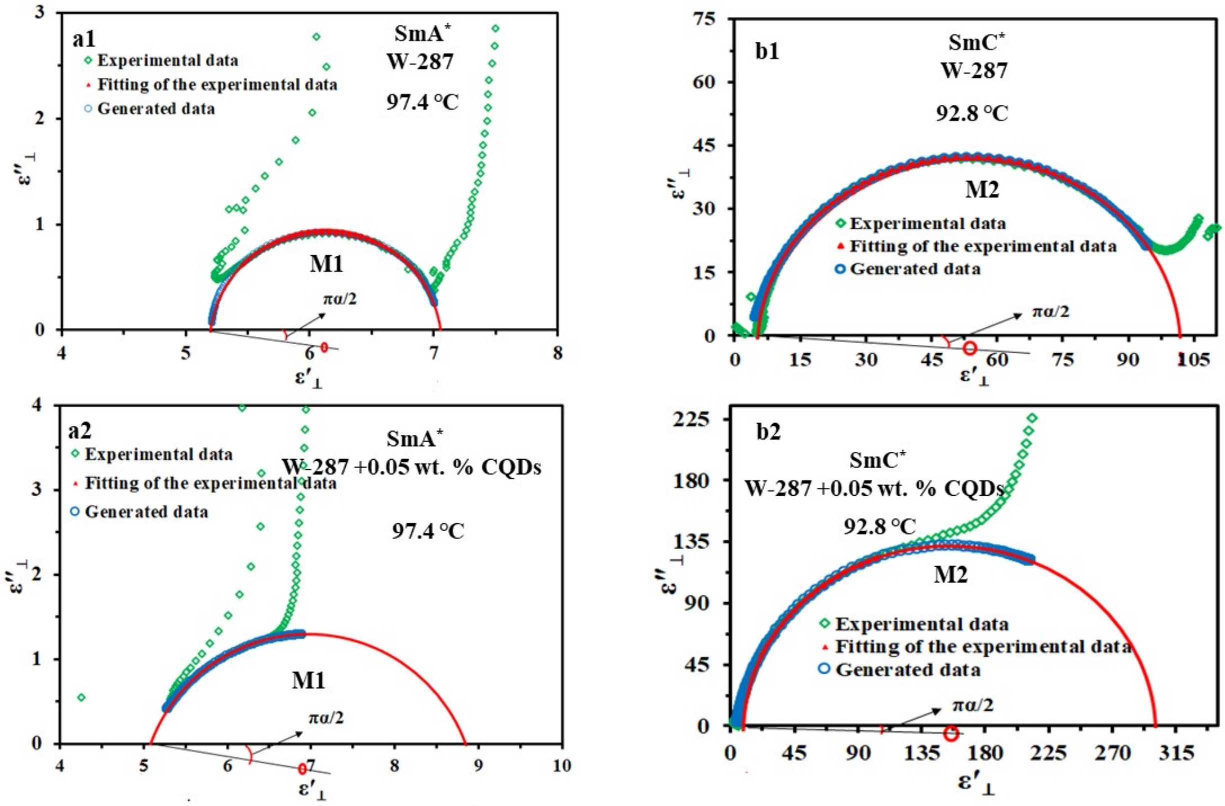

Figure S7. Cole–Cole plots showing the variation of loss $(\varepsilon'_{\perp})$ with permittivity $(\varepsilon'_{\perp})$ of the relaxation modes observed in the SmA* phase at 97.4 °C for (a1) pure W-287 and (a2) composite-1. In the SmC* phase at 92.8 °C for (b1) pure W-287 and (b2) composite-1, respectively.

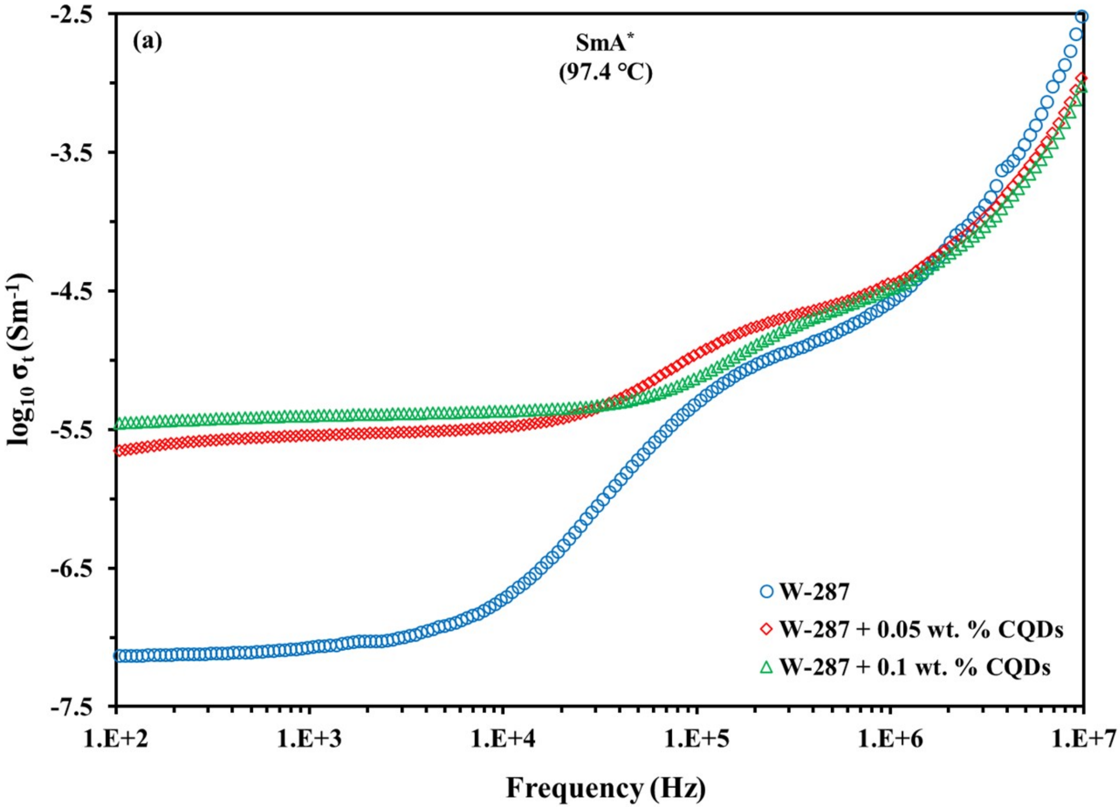

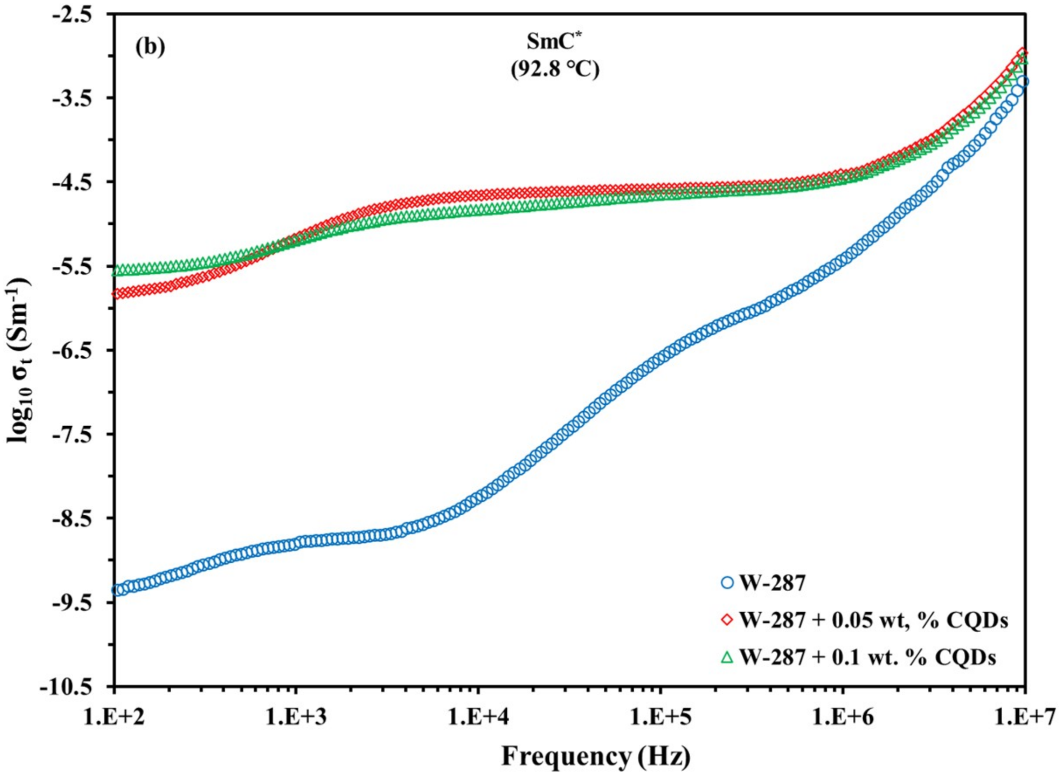

Figure S8. Variation of the total conductivity (σ_t) with frequency (Hz) of pure W-287 and its composites in (a) SmA* at 97.4 °C and (b) SmC* phase at 92.8 °C.